



Design and test to construct a magnetically driven piston pump for use in high-purity xenon experiments

Design und Tests zum Bau einer magnetisch getriebenen Kolbenpumpe für Anwendungen in hochreinen Xenon-Experimenten

Bachelorarbeit

von
Axel Buß

Themensteller: Prof. Dr. C. Weinheimer
Zweitgutachter: Prof. Dr. A. Khoukaz
Westfälische-Wilhelms-Universität Münster
Institut für Kernphysik
AG Prof. Dr. C. Weinheimer

Contents

1	Introduction	4
1.1	The XENON1T experiment	4
1.1.1	Dark matter	4
1.1.2	The need for high-purity / need for a Xenon pump	5
1.2	The EXO-200 experiment	7
2	Pump testing station	9
2.1	Construction	9
2.2	Testing a commercial pump	10
3	A magnetically driven piston pump	12
3.1	The existing EXO pump	13
3.1.1	Principle of the pump	13
3.1.2	Inner setup	13
3.2	New magnet configurations for a high flow, high pressure piston pump	14
3.2.1	Magnet configuration for strong coupling	16
3.3	Disposal of dimensions	17
3.4	Magnetic force simulations	18
3.5	Construction of magnet assemblies	20
3.5.1	Building the inner piston	20
3.5.2	Piston sealing and inner gas setup	24
3.5.3	Building the outer magnet ring	24
3.5.4	Mounting the outer magnets around the tube	28
3.6	Future construction	33
4	Measurement of force	34
4.1	Building a test setup	34
4.2	Comparison of simulation and measurement	37
5	Conclusion and Outlook	39

1 Introduction

Xenon has become an important detector material for radiation detection in particle physics and astrophysics[3]. The detection is done by scintillation and ionization of liquid xenon. The noble gas is used in experiments which require a low background e.g. experiments in astrophysics and particle physics. Two mayor experiments that are currently in development are XENON1T[4] and nEXO which will search for dark matter and the neutrinoless beta decay respectively. They will succeed the existing experiments Xenon100[19] and EXO-200[2].

In most modern physics experiments detectors of high purity are needed. High purity experiments like XENON1T or nEXO need a cleaning method to achieve a contamination below the ppb¹-level for electronegative impurities as they would have a negative impact on the charge/light yield. There is also the pursuit to achieve a high level of radio-purity by reducing the amount of radioactive components in the system. They would decay in the detector and thus produce unwanted signals. Usually that is done by a recirculation method through some kind of purifier. This already leads to the need for a pump with high requirements to purity, reliability, and performance.

As commercially available pumps do not satisfy the requirements, a new pump is in development by the Xenon dark matter group in the *Institut für Kernphysik, Universität Münster, Germany* in collaboration with the *Stanford University, USA*. The design, build, and tests to construct this pump are topic of this thesis.

1.1 The XENON1T experiment

XENON1T will be an experiment at the *Gran Sasso National Laboratory (LNGS)* to directly detect dark matter. It is supported by several international collaborating institutions. XENON1T succeeds the existing experiments XENON100 and XENON10. It will around 1 ton of liquid xenon as detector material and about 3 ton of xenon total.

The aim of research is to directly find dark matter.

1.1.1 Dark matter

In 1929 Zwicky[20] discovered that the velocity of stars within galaxies in the Coma cluster was different from calculations based on luminous (i.e. visible) matter. The rotational velocity of stars with higher radii to the center of spiral galaxies was higher than expected. Another unsolved problem were gravitational lenses which occurred in galaxy clusters. This is shown in figure 1. The green contours show the gravitational potential which are calculated by gravitational lensing. However the luminous mass is distributed mostly by hot gas that is shown in figure 1b. To solve this differences additional mass was proposed, as it would solve this problem. However, this mass has not been directly measured yet. Therefore the term *dark matter* was introduced by Zwicky[21], which describes an invisible mass which is spherical distributed around the galaxy centers.

¹ppb: parts-per-billion = 10^{-9}

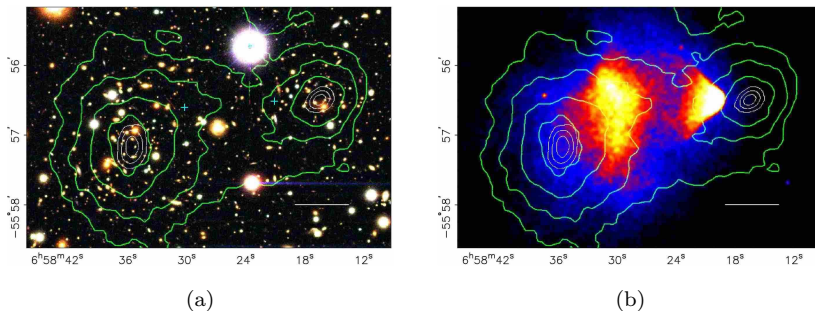


Figure 1: Photo of Bullet Cluster as evidence for the existence of dark matter from [9]

1.1.2 The need for high-purity / need for a Xenon pump

The XENON1T experiment is supposed to directly detect dark matter. Theories predict that dark matter consist out of WIMPs (weakly interacting massive particles). These particles only interact very rarely with nuclei. The reason why these particles does interact with baryonic(i.e. normal) matter at all, comes from the SUSY model. Due to the very rare interaction, an efficient detection with extremely low background is crucial for a unequivocal proof of dark matter.

The XENON1T experiment will use, as its predecessors, a time projection chamber (TPC). This is a cylindrical vessel filled with liquid xenon. At its ends, arrays of photomultiplier tubes (PMT) detect scintillation light which is emitted in the moment of nuclear recoil. This is called the S1 signal. Furthermore xenon atoms are ionized so that electrons are emitted as well. Due to an electric field, that is applied inside the TPC, electrons drift with constant velocity upwards towards a positive charged anode. In the gaseous phase above the surface of the liquid xenon, the electrons are accelerated by a stronger electric field. At high velocities the electrons can excite xenon gas atoms which produces scintillation light by photoluminescence. The amount of emitted light is proportional to the amount of electrons. This light is also detected by the PMTs and is called the S2 signal. By the drift time and the 2D position of the S2 signal the 3D position of the initial can be reconstructed. A direct detection of the electrons is due to their little amount of charge not possible.

In figure 2 the principle of the TPC and the accordingly expected waveforms are shown. As the ratio between the S1 and the S2 signal is different for WIMPs and γ -rays, a discrimination can be done. This way background signals can be

sorted out.

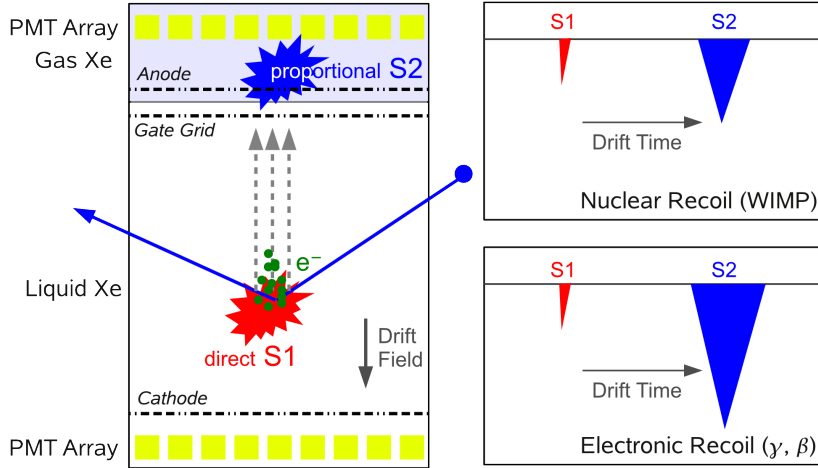


Figure 2: Left: schematic principle of a two-phase TPC. Right: schematic waveforms for S1 and S2 signal for WIMPs and γ -rays. Image from [19]

This drifting process is only possible with a high purity within the liquid. Electronegative impurities like oxygen or nitrogen absorb the electrons, thus attenuating the S2 signal. In order to prevent that, the gas has to be cleaned with a getter. It absorbs most of the to be expected elements by a chemical reaction. The products of this reaction are kept away from the rest of the gas system. Noble gases do not react and therefore can not be filtered out with this method.

Radioactive impurities are also a problem for the experiment. Mainly ^{85}Kr is an isotope, created by nuclear bomb tests in the last century, that makes it difficult for the experiment as it cannot be filtered out easily. Furthermore it is a beta emitter with an endpoint energy of 687 keV, which are in the same energy region as the expected recoil energies of dark matter induced scintillation. This would create a tremendous amount of background signals, making the identification of actual dark matter signals impossible. Another issue is contamination with radon(Rn). As it also induces unwanted signals, a low concentration is desired. To decrease the already low concentration of krypton within xenon a distillation column is being developed in Münster. Unfortunately this method is not able to reduce the radon concentration.

Furthermore, signals that do not come from a certain zone in the center of the TPC are rejected, as they are more likely to be background. This internal shielding is done to rule out signals, that come from radioactive impurities from outside of the detector.

The estimated sensitivity in comparison to other dark matter experiments is shown in figure 3. Only in the area above the curves WIMPs can be detected by the accordingly experiment. The grey area in the bottom right is a theoretical prediction where WIMPs can be expected[8]. XENON1T will therefore have an increased sensitivity to the sensitivity for WIMP-Nucleon cross section by two

orders of magnitude.

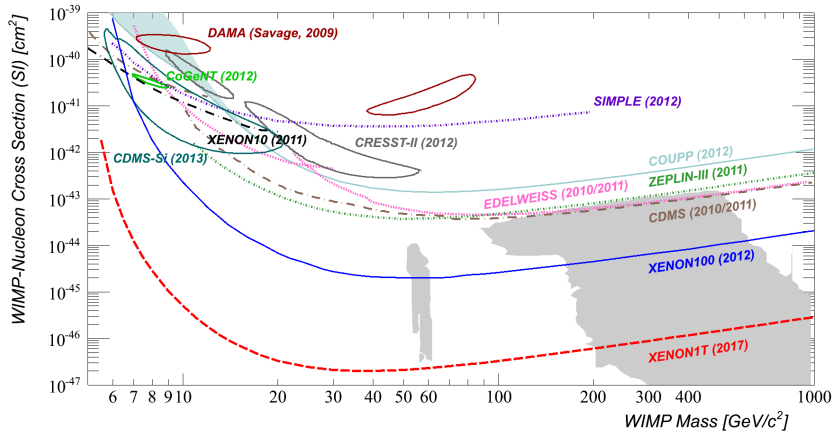


Figure 3: Sensitivity for XENON1T(expected) and other experiments.

1.2 The EXO-200 experiment

The *Enriched Xenon Observatory* (EXO) is an experiment to detect the neutrinoless double beta decay ($0\nu\beta\beta$) of ^{136}Xe . The isotope ^{136}Xe decays by double beta decay into ^{136}Ba . Like the XENON1T experiment it uses xenon as detector material. However Xenon itself is the research object, too. Even-even nuclei² cannot decay by the ordinary beta decay as it is energetically forbidden. However a double beta decay is allowed by the standard model, although it is extremely rare. This process is well known for the ordinary double beta decay which emits a neutrino and an anti-neutrino. The neutrinoless double beta decay has not yet been observed but some theories predict it. A successful discovery of the neutrinoless double beta decay would prove that neutrinos are Majorana particles. This means neutrinos are its own anti-particles. Furthermore the not yet known mass of neutrinos could be measured at the same time. This is a current topic of research for various other international experiments.

The experiment's construction[5] was done with extreme attention to purity at all times. Every component was carefully picked and tested to minimize any contamination by radioactive impurities[16]. The reasons for the extreme purity demands are the same as for the XENON1T experiment. However, as the magnitude of energy is very different from the expected dark matter signals, ^{85}Kr is not the major problem. Electronegative impurities do have the same impact as for XENON1T, though. As the XENON1T experiment it uses a TPC as detector. However there are several differences in design which follow from the different aim of research. The TPC does not need an amplification for the ionizing signal, as the Q-value³ is 2457.8 keV. It is hence possible to directly measure the much higher amount of electrons (i.e charge) without a gaseous phase for second scintillation which was used for the XENON* TPCs. This allows a horizontal setup, which is shown schematically in figure 4.

²Even-even nuclei = nuclei with an even number of neutrons and an even number of protons

³The Q-value is the amount of energy released by a reaction

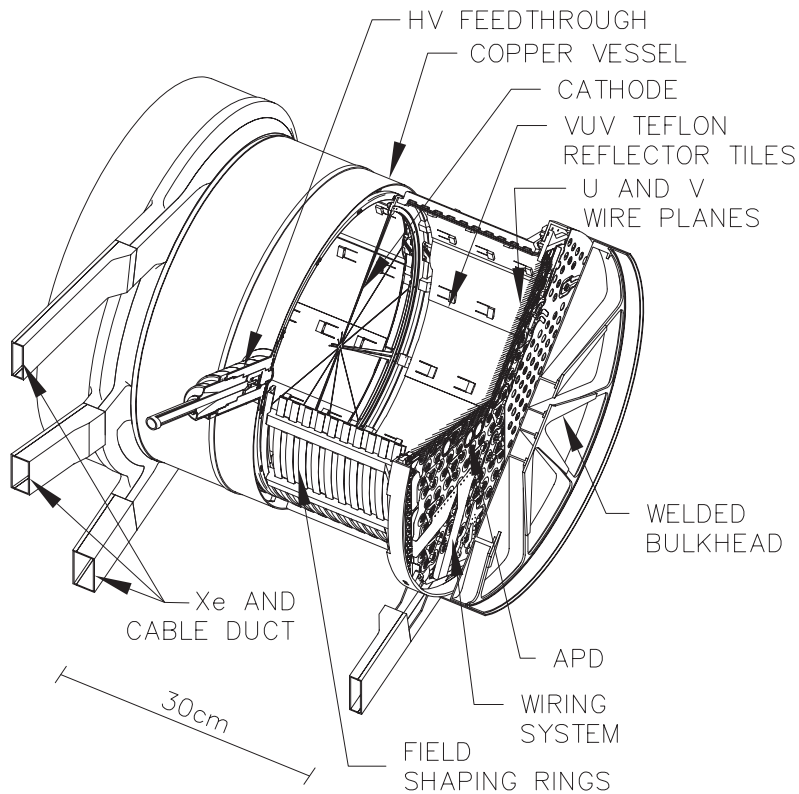


Figure 4: Cutaway view of the EXO-200 TPC with the main components identified. Image by [5]

The detector is a double TPC, having a wire cathode in the middle and two wire grids on each side. This minimizes the surface-to-volume ratio while maintaining a practical geometry. The wire grids at both ends are made of 2 separate parallel wire array each. These are rotated 60° against each other and are mounted with 6 mm distance. The wires closer to the cathode are called *V-wires* and the others *U-wires*. At each end of the cylindrical vessel an array of 234 large area avalanche photo-diodes (LAAPDs) is mounted. As they combine high quantum efficiency for the scintillation light with ultra-low levels of radioactivity they were preferred over photomultiplier tubes.

When a ^{136}Xe nucleus inside the to 80.6% enriched⁴ xenon decays, light is emitted which is almost immediately detected by the LAAPDs. Additionally electrons are emitted which drift due to the voltage between cathode and the U/V-wire grid towards the end of the vessel. As they pass the V-wires a signal can be measured by induction. Then the total charge is collected in the U-wires. Low-noise electronics can determine the individual wires that produced a signal. The 2D position of the electrons is reproducible by the angle of 60° . By knowing the time difference between the scintillation light and the ionization signal the

⁴ ^{136}Xe is enriched with the same technique as ^{235}U .

3D position of the initial decay can be calculated. This allows a discrimination so that signals near the surface can be ignored as they are more likely background. Electronegative impurities would absorb the electrons, attenuating the measured current at the wire grids. A high purity is crucial to achieve best detector efficiency.

EXO-200 has not yet discovered evidence for the $0\nu\beta\beta$ decay, but confirmed the half-life of $T_{\frac{1}{2}}^{0\nu\beta\beta} = (2.23 \pm 0.017 \text{ stat.} \pm 0.22 \text{ sys.}) \cdot 10^{21} \text{ yr}$ [6]. EXO-200's successor *nEXO* (next EXO) will benefit from the technological developments which made this experiment possible. This includes the EXO-200 pump (see 3.1) which was developed for this experiment.

2 Pump testing station

To satisfy the performance needs of *nEXO* and *XENON1T*, a pump with a flow of 100 slpm and a maximum differential pressure of 2 bar is required. To ensure that these specification can be met and to measure the performance of various recirculation pumps, a pump test station has been built for systematic characterization. The pump test station is designed to measure the pressure at the inlet and the discharge of a pump as well as the flow.

2.1 Construction

The setup of the pump testing station is shown schematically in figure 5. The parts are connected with 1/2" electropolished pipes and VCR connectors. This eliminates possible contamination. The flow controller (*mks 1579 B*[12]) is used as a flow meter. The vacuum pressure sensor PI03 is a *mks 972B DualMag*. The pressure sensors PI01 and PI02 are *PTU series pressure transducers* from *Swagelok*[14]. The RGA is a *Quadruvac Q100* from *Leybold-Heraeus GmbH*.

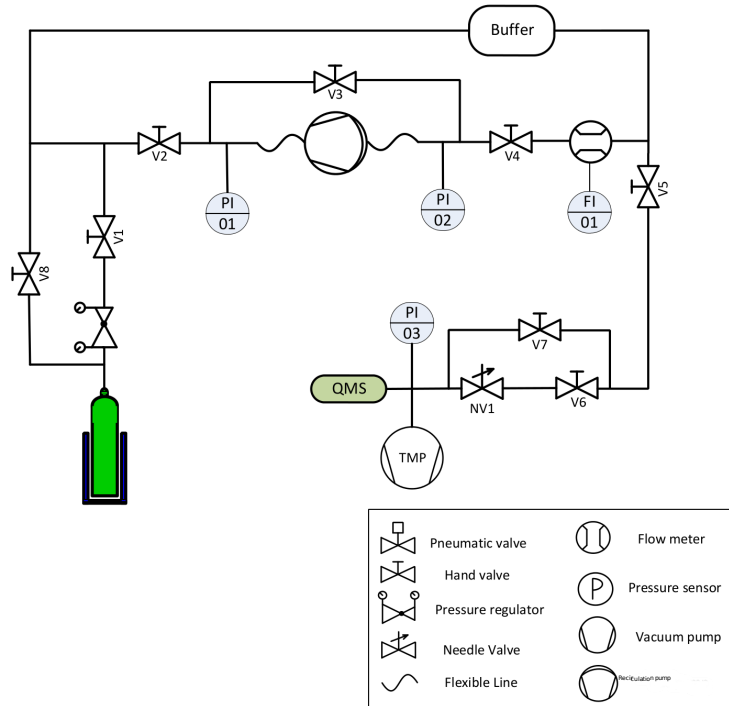


Figure 5: Flowchart of the pump test station. Image by [15]

Gas is recirculated through the upper lines by the testing pump in the center. The pressure sensors PI 01 and PI 02, as well as the flow controller FI 01 are monitored/controlled by a LabView program.

For initial operation the system is evacuated through the TMP first (roughing pump not shown). All valves except V1 and V8 are open at this time. Then valve V5, V6, and V7 are closed and the system is filled with Argon up to 3 bar through V1. It can be used as it has similar properties as Xenon which is not used for practical reasons.

During the test V5 and V6 can be opened to provide a connection to the residual gas analyzer(RGA) (in figure 5: QMS). Through the needle valve NV1 only a small amount of gas can flow so the pressure in the chamber behind remains at a 10^{-5} mbar level. However the needle valve was not yet available so the valve V7 was so far just opened slightly and then closed again. The streamed in gas can now be analyzed by the RGA. If there is contamination by the pump, they can be identified by this method.

2.2 Testing a commercial pump

The properties of interest of a pump are the differential pressure and the associate flow. At a low differential pressure the flow can be apparently higher than at a high differential pressure. This connection for a commercial available

pump is topic of this section. The long term stability which corresponds to the thermal stability has also been investigated.

The pump described in the following is a custom made pump called QDrive from the company *CHART*. It uses a lubricant free piston to compress gases preferably argon. The motors are two coils which moves the ferromagnetic pistons inside a tube. For the motors a oscillating current is provided by a *PowerFlex 700* from *Allen-Bradley*[1]. The pump can be run up to a voltage of 118 VAC at a frequency from 50-70 Hz. The mechanism behind this pump is a damped high frequent oscillator. So the performance is dependent on the resonance frequency. At already moderate loads it needs a cooling water supply.

For systematical performance characterization, the flow was measured against the differential pressure at different frequencies. In all tests the voltage was 110 V, so almost at the maximum voltage of 118 V. All tests have been done with the same argon gas at 2.2 bar initial inlet pressure. All valves were closed except V2 and V4 at this time. By slowly closing V4 the pressure at the discharge of the pump (PI 02) rose. The buffer volume ensures a nearly constant pressure at the inlet of the pump (PI 01). While the valve V4 closed and the discharge pressure rose, the flow measured by FI 01 decreased. Every 20 seconds the valve was closed further until the flow decreased to zero. A Labview program averaged 10 measurements over 20 seconds and saved it into a data file with the accordingly standard deviation. The result for various frequencies is shown in 6. The measurements show that a higher frequency results in a higher

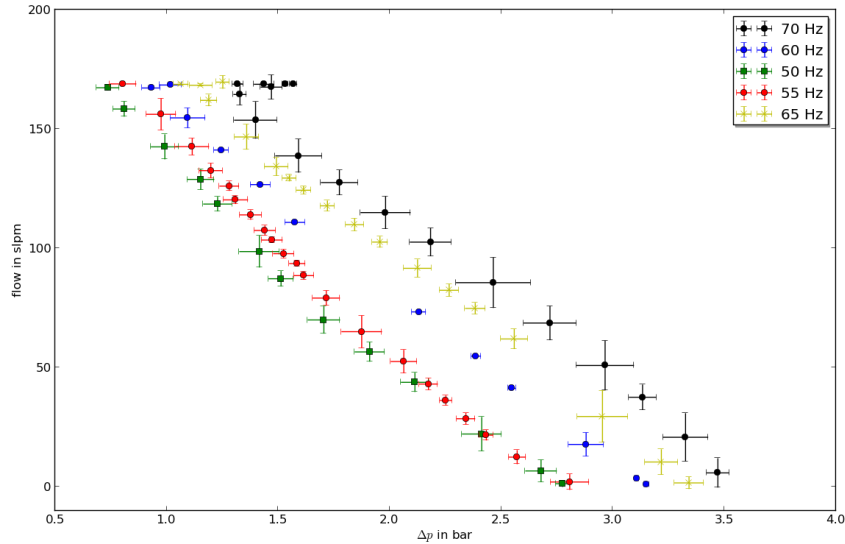


Figure 6: Flow against differential pressure at different frequencies and 110 V AC

flow at a given differential pressure. Also the maximum differential pressure is with 3.5 bar highest at 70 Hz. It turned out that the set voltage of 110 V was not applied to the pump at lower frequencies. The actual voltage and current that was displayed on the controller are shown in table 1. It is not known why

the controller could not apply the set voltage to the pump.

Table 1: Power consumption at different frequencies

Frequency[Hz]	Voltage[V]	Current[A]
50	72	8.1
55	92	9.0
60	102	9.3
65	109.9	8.6
70	110	9.0

To measure possible contamination by the connected pump, the pump testing station is equipped with an RGA. This quadrupole mass analyzer can measure the mass/charge ratio of molecules. Most of the molecules are single ionized, so that it is common to say that the mass is measured. An exemplary mass spectrum is shown in figure 7. It shows a mass spectrum of the gas system after 3 days of cleaning argon with a getter. However the Peaks at amu 28 and 2, which represents N_2 and H_2 respectively and to which masses the spectrum was calibrated, show a still higher concentration than for argon (amu 40). The other peaks refer to water (H_2O , amu 18), oxygen (O_2 , amu 32), ethanol (amu 46) and their fragments. Ethanol is there because it was used for cleaning the pump and other parts before mounting them on the system.

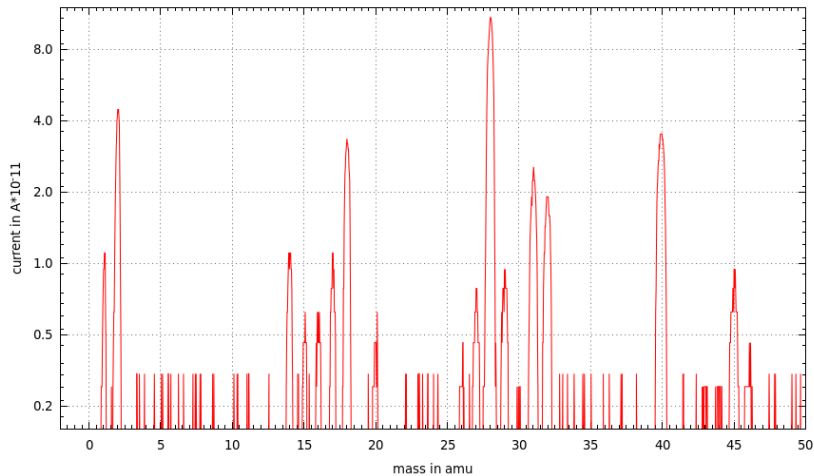


Figure 7: Mass spectrum of the gas system with Q-drive connected after 3 days of recirculation through a getter.

3 A magnetically driven piston pump

Existing pumps operate at the edge of the specifications required by nEXO and XENON1T. The required flow of 100 slpm and pressure of 2 bar would be possible by the use multiple pumps. However, long term tests made in Heidelberg with the Qdrive indicated a not insignificant contamination with

Rn. Multiple pumps would provide an even higher contamination. Therefore a single pump, proving the needs for purity and performance is therefore desirable.

A new pump is being developed for the use in recent high purity xenon experiments. It is designed to fulfill the requirements of nEXO and XENON1T, especially in terms of purity, reliability, and performance. A magnetically driven piston design ensures high purity, long term stability, and in case of a failure, no contamination to the gas system.

3.1 The existing EXO pump

The pump design is based on the EXO pump of Leport et al.[17]. It was designed for use in the EXO-200 experiment. The gas recirculation is done by a magnetic piston which moves inside a tube. However in contrast to the Qdrive the drive is not done by coils, but with an outer magnet ring which is then moved by a linear drive. Also, the EXO pump cannot be described as a damped oscillator. As the movement of the piston is rather slow, it is a magneto-static issue. In the whole building process, every part was carefully chosen to not bring radioactivity into the system.

3.1.1 Principle of the pump

For the recirculation of xenon other types of pumps had been tested. Even double containment, all-metal bellows pumps which were designed for long term durability tend to leak after a month of operation[17]. That is why a piston design was chosen. The piston is driven in a cylinder (i.e. tube) by an outer ring magnet which is magnetically coupled to the piston. This ensures that, there is no contact of the air to the inner gas system. Even if a leak between the piston and the cylinder occurs in long term, the xenon will not be contaminated as it is still separated from the atmosphere.

A schematic view of the pump is shown in figure 8. The piston with the inner magnet moves along the tube and displaces the gas. The drive is a linear motor. Reed valves at the end allow flow only in one direction as marked by the arrows. Additional ports for vacuum pumping are needed because the reed valves are closed at too low pressure differences.

Apparently the flow is proportional to the speed of the piston and the maximum differential pressure is limited by the maximum coupling force.

3.1.2 Inner setup

To achieve the best possible coupling between piston and the ring magnet simulations were made to find the optimal length of the magnets. Lengths of 2.5, 5.1 and 7.6 cm were considered as the diameter for the cylindrical piston magnet with 5.1 cm was fixed, as well as the inner and outer diameter of 7.6 and 10.2 cm of the outer ring magnet respectively. Accordingly, the gap between piston magnet and ring magnet is 7.5 mm.

The result of the simulation is shown in figure 9. It turned out that magnets of 5.1 cm have a maximum force of 480 N while 2.5 cm long magnets have a maximum force of 300 N. However, 7.6 cm length have no noticeable advantage over 5.1 cm long magnets. Therefore the 5.1 cm magnets were chosen. Some of

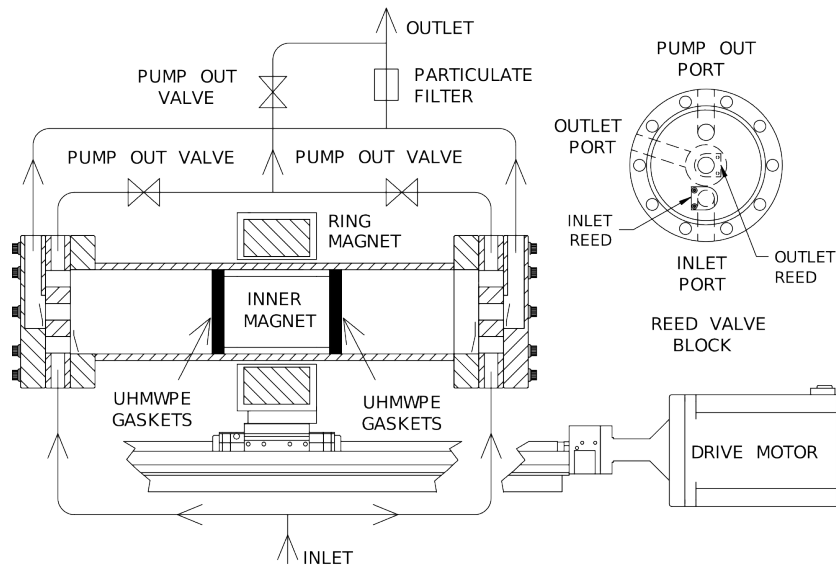


Figure 8: schematic setup of the existing EXO pump. Image from [17]

the strongest available neodymium magnets were picked, to achieve strongest coupling.

As a lubricant cannot be used to reduce the friction between piston and cylinder has to be reduced by a different method. As mentioned above, a leaking seal is not as problematic it does not contaminate the system. It reduces the efficiency of the pump, though. This lead to a dynamic design, which compensates wear of the seal. By using a gasket that is pushed against the cylinder wall with a constant force a gap cannot arise. The method is shown in figure 10. The edge of the pressure surface is conical shaped at a 45° angle. A spring washer presses it against the gasket with a constant force of 20 N (1 N/cm). One gasket is vented through, as the volume between both would be hard to evacuate otherwise. The piston magnet is completely isolated inside a laser-welded container.

For this tensioning mechanism the right material is crucial. Intense test with several polymers were made. The material with the least wear was ultra-high-molecular-weight polyethylene (UHMWPE). For minimum outgassing the gaskets were baked in a N_2 -purged oven for 200 hours at 93°C . This is the only part which comes in contact with the gas in the whole pump and that is not made out of metal.

3.2 New magnet configurations for a high flow, high pressure piston pump

The existing EXO pump has a output of maximal 16 slpm with a differential pressure of up to 1 bar. With the aim of about 100 slpm flow and 2 bar maximum differential pressure the dimensions of the EXO pump are, even with a different magnet configuration (see below), insufficient. Therefore new dimensions had to be found, concerning costs, delivery time for parts and manufacturable restrictions.

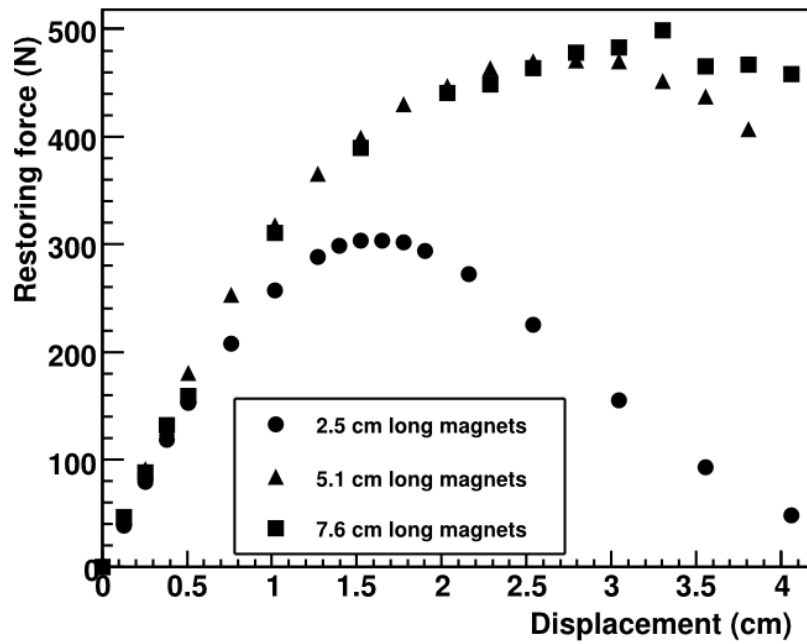


Figure 9: Restoring force of inner magnet depending on displacement for different magnet lengths. Image from [17]

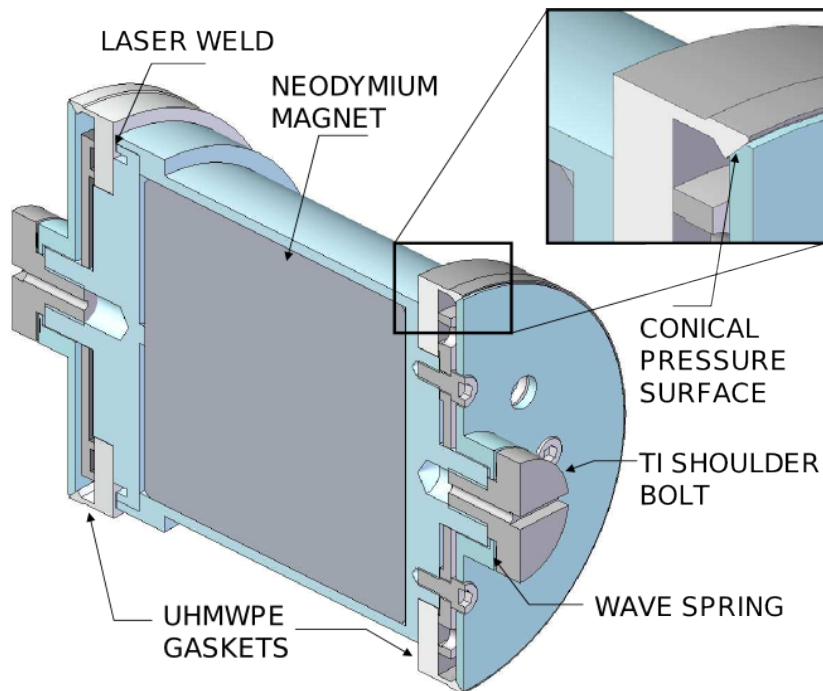


Figure 10: A view of the piston with sprung UHMWPE gaskets. Image from [17]

3.2.1 Magnet configuration for strong coupling

In order to increase the coupling force between the piston and a pump new magnet configurations were considered by E.Brown[7]. This is necessary to increase the force and with it the maximum differential pressure. The primary idea is to have multiple magnets with alternating polarity. This is schematically shown in figure 11. With this setup the total force between the magnets does not only add, but increases by the additional force through cross coupling, too. As shown in figure 12 the highest field strengths occur in the middle between the gaps of the magnets on the right and on the left. Simulations of [7] showed that 3 magnets of 2.5 cm length each deliver a higher coupling force than two 7.6 cm magnets.

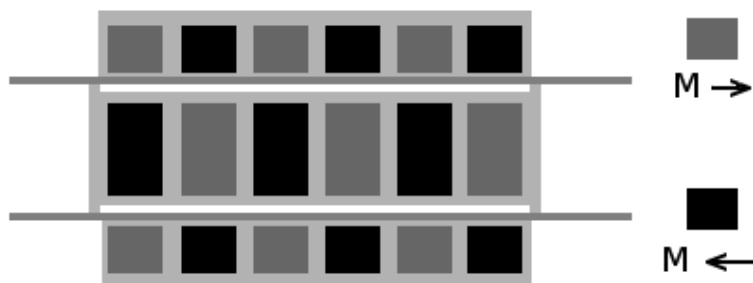


Figure 11: Schematic arrangement of magnets. Image by [7]

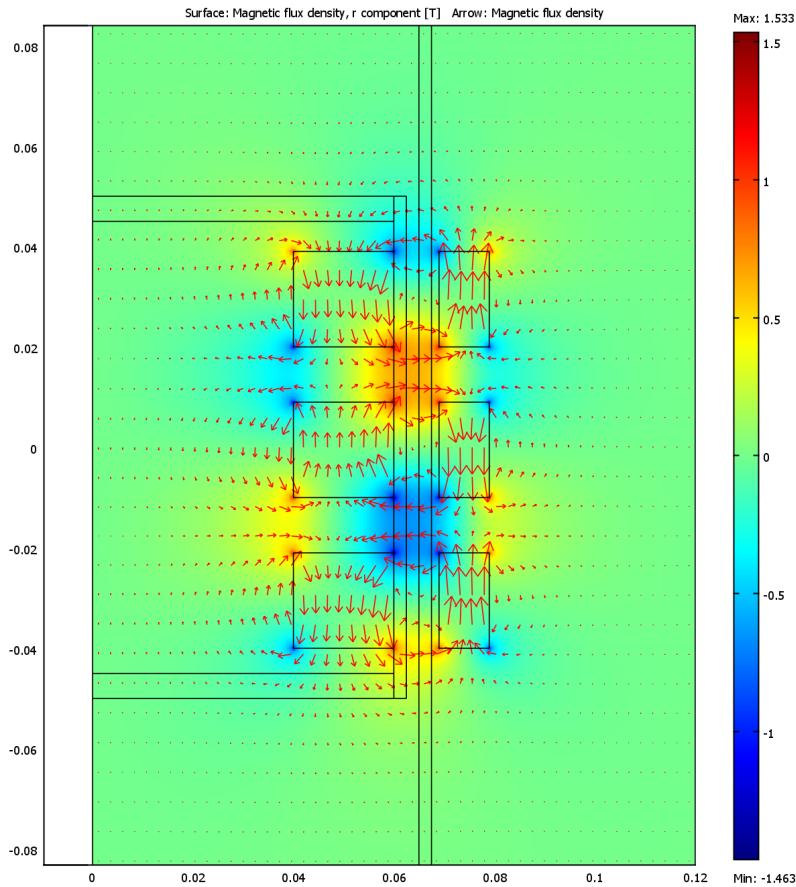


Figure 12: Schematic arrangement of magnets with magnetic field simulation (r -direction).

3.3 Disposal of dimensions

The first thing which had to be fixed was the size of the inner magnet rings. In order to achieve the aim for flow, a larger volume will be needed. The choice came to an diameter of the inner magnet rings of 120 mm. From this follows even larger rings for the outside. The exact size for the inner diameter of this outer rings depend on the total gap between the inner and outer magnets. This gap consists of the thickness of the tube and the the case for the inner magnets, as well as the gaps to the tube. Because of the stronger coupling between the magnets a smaller gap is desirable. In collaboration with Stanford University that will build the gaskets, a gap of 9 mm was expected to be possible. This means the outer ring has to have an inside diameter of 138 mm. For the length 20 mm were chosen.

Another important aspect is the magnet material. It should have a high magnetic flux density to produce high forces and it should have the capability to operate at moderate temperatures. If it hadn't the latter quality the pump

frequency could possibly be limited to keep the magnets under their maximal operation temperature.

The range of companies who can produce magnets with this unusual large sizes and special requirements is very limited and the prices are accordingly high. Luckily one manufacturer[10] had some spare magnets of an old order in stock by chance.

For the outer ring no fitting ring magnets could be found for reasonable prices and without delivery times of several months. For this reason a design made by segments of 10x10x20 mm bar magnets were chosen. They will need to be arranged as a ring with small gaps around the tube by an additional assembly (see 3.5.3). This gives a good compromise between costs and performance. Furthermore, as the final outer diameter of the tube wasn't fixed at this time, this construction gives some flexibility considering that the number of magnets could still be varied.

3.4 Magnetic force simulations

Dependent on the coupling force the performance of the pump can be calculated. Therefore simulation were calculated using COMSOL[18]. The basic setup was simplified to a radial symmetric structure⁵. In other words, the individual bar magnets for the outer ring are calculated like a single ring. The resulting differences have to be compensated.

COMSOL was used to simulate the magnetic field of the inner piston magnets. The coupling force was then calculated by a ROOT script.

The force applied to a magnetic dipole $\vec{\mu}$ is

$$\vec{F} = -\nabla(\vec{\mu} \cdot \vec{B}). \quad (1)$$

The force to a magnet consisting of dipoles is in cylindrical coordinates

$$\vec{F} = \iiint_{V_{\text{magnets}}} -\nabla(\vec{\mu}(r, \phi, z) \cdot \vec{B}(r, \phi, z)) r dr d\phi dz \quad (2)$$

The dipole moment $\vec{\mu}$ is assumed to be independent of its position vector and only orientated in z-direction.

$$\vec{\mu} = \begin{pmatrix} 0 \\ 0 \\ 1.38\text{T} \end{pmatrix}$$

1.38 T is the magnet flux density inside the outer magnets. The value was given by the manufacturer. The \vec{B} -field is independent of ϕ as it is radial symmetric. From that follows that the scalar product

$$\vec{\mu} \cdot \vec{B} = 1.38 B_z$$

The integral from (2) simplifies to

$$\vec{F} = 1.38\text{T} \iiint_{V_{\text{magnets}}} -\frac{dB_z}{dz} r dz dr d\phi \hat{z} \quad (3)$$

⁵This was done because the used version of COMSOL cannot do 3D magnetic simulations. Exact simulations would also need a much bigger amount of effort and computer time without big physical advantages as the magnetic field is axial symmetric to lowest order.

For a ring magnet with rectangular cross section this can be easily solved. However, with bar magnets as they will be used, the borders of the integral are coupled together making the solution much more difficult. It is much easier to replace $rd\phi$ by $R_{\text{inner}}d\phi$ and keeping the borders as they are. This works because the volume element does not grow with the radius for a circle of cuboids. Actually $\int_0^{2\pi} R_{\text{inner}}d\phi$ is already known. It is the sum of all⁶ magnet lengths around the circle.

$$\int_0^{2\pi} R_{\text{inner}}d\phi = 40 \cdot 10 \text{ mm} = 0.4\text{m} \quad (4)$$

The formula comes to the final form

$$\vec{F} = 400 \cdot 1.38\text{T} \int_{R_{\text{inner}}}^{R_{\text{outer}}} \int_{z_{\text{lower}}}^{z_{\text{upper}}} \frac{dB_z}{dz} dz dr \hat{z} \quad (5)$$

The integral is then solved numerically using the simulation data of COMSOL.

The result is shown in figure 13. The maximum force of about 2870 N for the bar magnet configuration occurs at a displacement of 15 mm. The maximal differential pressure Δp is given by $\Delta p = \frac{F_{\text{max}}}{A}$. With the piston cap area $A = \pi \left(\frac{d}{2}\right)^2 = \pi \left(\frac{127 \text{ mm}}{2}\right)^2 = 12676 \text{ mm}^2$, the maximal achievable differential pressure is 2.27 bar.

To verify that the bar magnet configuration is not dramatically lower than the ring magnet configuration a second simulation has been performed. The result is also shown in the figure. The maximum force for the ring magnet configuration is 3280 N, so 14% higher than the bar magnet configuration.

The force gain by the ring magnet design is comparatively small. The amount of additional material, which lacks in the gaps of the bar magnet configuration is 16% higher. So the possible gain in force is even lower than the needed amount of additional material.

⁶There are 40 magnets in one circle. See 3.5.3

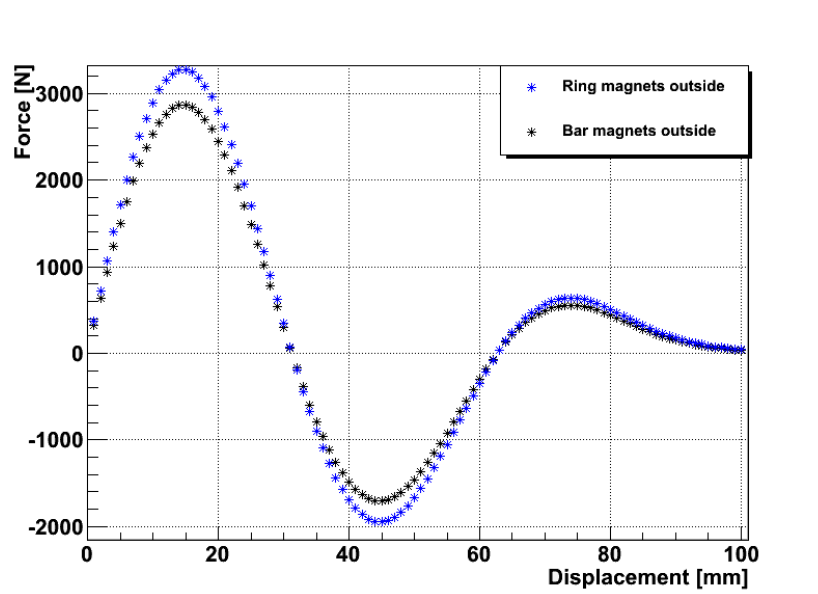


Figure 13: Simulated restoring force at a given displacement for ring and bar magnet configuration. The maximum force occurs at a displacement of 15 mm. At about 31 mm the force direction flips. At about 62 mm displacement there is another stable equilibrium. The magnetic material is the same for both configurations.

3.5 Construction of magnet assemblies

Due to the strong magnets used for this pump, several difficulties occurred during the construction process. Some of them were foreseeable, others were unexpected. This comes from the unintuitive strong forces which dramatically increase at low distances to any magnetic material. This would have made the whole process potentially dangerous, if several precautions hadn't been considered first.

3.5.1 Building the inner piston

The piston which later displaces the gas contains three inner magnet rings. These are made out of 4 mm thick rings which have to be stacked to a magnet ring of 20 mm height. Because of the high fragility it was no solution to just bring them close together and let the magnetic forces do the rest. This would have ended in scattered pieces for sure. It turned out that the probably easiest, fastest, and (for the magnets) safest way to do the stacking was by hand on a table. This is shown schematically in Figure 14. With more magnets on the stack, the coupling force rises noticeably, making the process even more difficult. The most dangerous moment is, when the force, needed to push them one over the other (Fig. 14c), suddenly vanishes and the magnets slide into full overlap (14d). Without exaggeration the force is strong enough to cause bruises or even fractures. A supporting frame made out of Kanya[11] profiles was tried also,

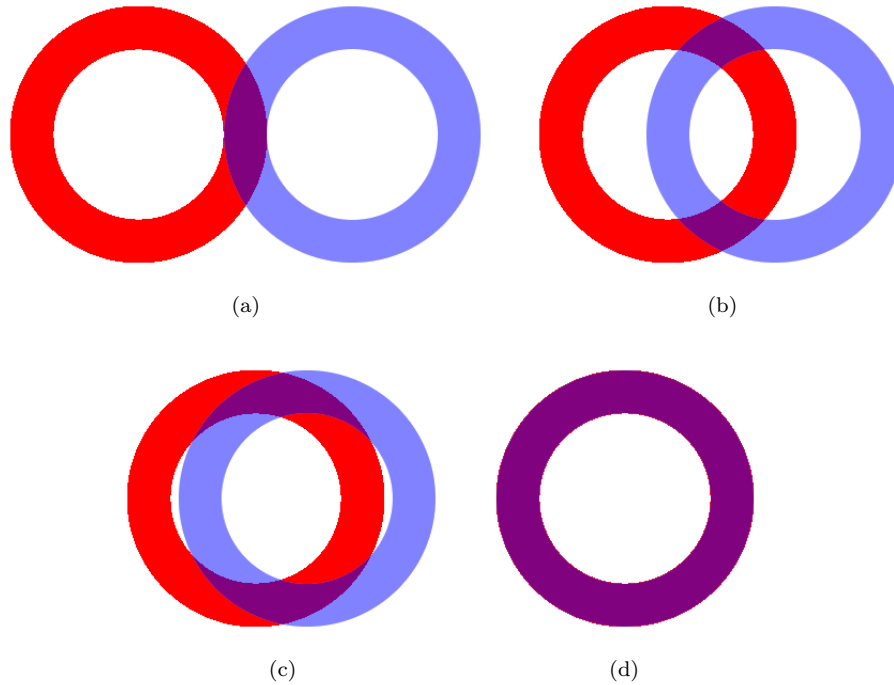


Figure 14: Bringing the ring magnets together. First the rings are put together like shown in a). They stay in this position by themselves. Then they are pushed from the sides against a small repulse force b). At an overlap approximately like shown in c) the repulse force turns into an attracting force and the magnets slide into full overlap d).

but this led to a fracture of two rings. Since replacements weren't available, one stack had to be replaced by 4 pieces of 5 mm rings.

The piston contains three of the magnet stacks shown above. There are some requirements that have to be solved by the design. First, the magnets have to be kept at distances of 10 mm in z-direction. Therefore the construction needs to withstand the magnetic forces. Second, the piston magnets must not move away from their common axis. As the piston needs to be sealed in a tube (see next chapter) they must align so that the tube fits over it. Third it must not affect the magnetic field in a negative way. Finally, the construction must not tend to damage the magnets during the building or in long term during the movement in the pump.

To fulfill these requirements the following design was chosen. For the top and the bottom there will be end caps made of aluminum. Between the magnet stacks there are aluminum spacers. These parts warrant the distances in z-direction. In the center of the rings there is a cylinder, that aligns the rings on a common axis. The assembling is visualized in figure 15. The bottom end cap is fixed to the

base plate. The first magnet and spacer can be put over the inner cylinder easily, as no other magnetic parts are in range. The second ring magnet is then put into the not entirely closed tube, which ensures no movement but in axial direction. As the magnetic polarity is opposite to the first, the magnet is repelled. For the possibility to push it down from two sides, holes were cut into the back of the tube. Due to the high forces (see below) it was not possible to push the magnet all the way down. After another spacer the third magnet was pushed down with the end cap like shown in fig. 15b. At position 15c the setup was stable enough to unhand the second magnet, which had to be held until then. After tightening the centered M20 nut, the outer tube could be removed and 4 M8 threaded rods were used to hold the piston core together for good. After that the M20 threaded rod could be removed.

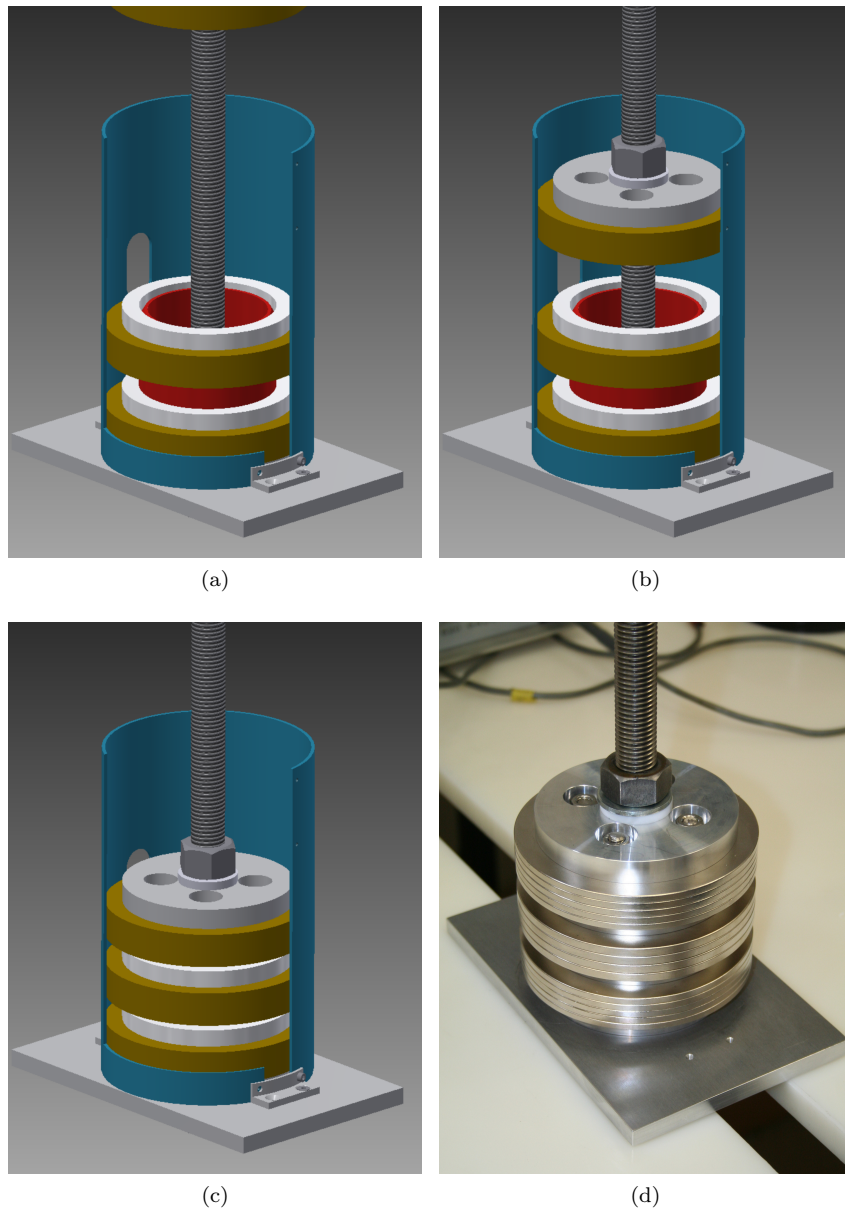


Figure 15: Assembling the piston core. An aluminum tube (blue) ensures axial alignment of the ring magnets (brown) before the are put over an inner cylinder (red). Spacers (white) keeps the ring magnets at 10 mm distance. For better visibility, the tube has been cut in these views. d): Constructed piston core.

As the magnet stacks must be placed in repulsing orientation a simulation in COMSOL was done before to determine how strong this force would be. This gave an idea for the force that could be expected and therefore how the magnets will be held together. The result of the simulation is shown in figure 16. The force at the final distance of 10 mm is about 800 N. To control the construction

at these high forces the method above was developed to prevent injuries and damage to the magnets.

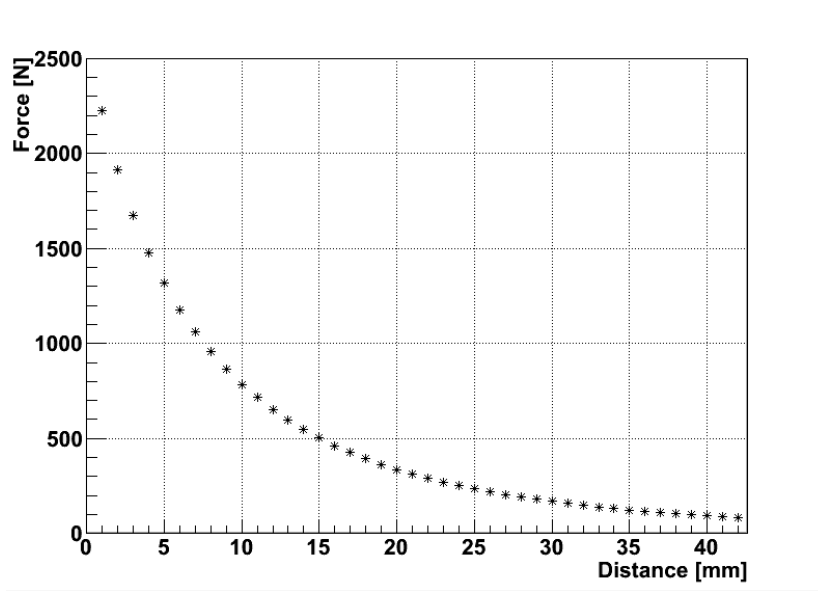


Figure 16: Simulation of force for repelling piston magnets

3.5.2 Piston sealing and inner gas setup

As already mentioned before the pump must not contaminate the system in any way. This automatically excludes any form of lubricant as it would contaminate the system. To ensure a reliable operation, the friction between the piston and the inner side of the tube must be reduced by a different method. As the gaskets for the EXO-200 pump out of UHMWPE have been approved, the design was adopted for this pump. The principle was already described in 3.1.2 and does not differ for this pump. A photo of the not yet finished assembly is shown in figure 17. It was done by Stanford University.

3.5.3 Building the outer magnet ring

With the piston settled, the construction for the outer ring needs to be considered. This will move the piston inside the tube by magnetic coupling. A strong coupling is obviously essential for good performance.

In the previous section we have seen that the casing and the gaskets need some space. With this space fixed, the size for the tube could be chosen. The choice came to a tube with 4 mm thickness and an outer diameter of 135 mm.

As a result of that the construction's inner diameter was designed with a 136.4 mm inner diameter and hence a 0.7 mm gap to the tube. The bar magnets need to be as close as possible to the piston magnets because the coupling force decreases dramatically with higher distances.



Figure 17: Inner piston magnets with container, made by Stanford University

The magnets are held within a custom made aluminum holder (see figure 18). To achieve sharp corners in the sockets for the bar magnets the piece was cut out of an aluminum block by wire cutting. This warrants small tolerances so that the magnets cannot move inside their socket. On the bottom side the magnets are held by an aluminum plate which has an 0.8 mm thick edge to prevent movement to the inside. On the top side they are tightened by a washer and a M6 screw each. This method minimizes the risks of moving parts and gives much control. Additionally each next magnet stays in place by itself (like the third one in figure 18) when it's at its final position. Before that the already positioned magnets drag the current to be placed magnet away from its target. This makes the process rather difficult, but not so much that an originally considered assistant tool was needed. To reduce this annoying influence, every second magnet was placed first. The other magnets can then be put into the vacancies. Of course the attracting force is still there, but it is not single-sided any more. This made the process a bit easier. Additionally the initial putting of every second magnet is a lot easier and therefore safer.

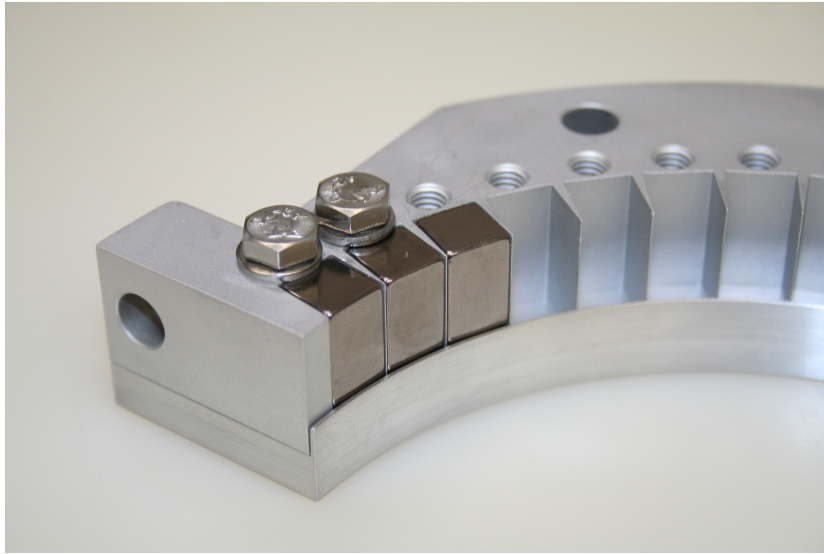


Figure 18: Outer magnet holder. The magnets are held tight within the form with a particular washer. The third one stays in an unstable equilibrium because there is no force in up-direction.

With all holders loaded the next step is stacking the half-rings with alternating polarity. This process is equal to the building process of the piston which was described in the previous chapter. As shown in figure 19 the middle magnet holder levitates about 6 cm above the bottom one. As with the piston a tightening of it first was forborne. Instead the third magnet holder was placed above, as shown in figure 20. With the same threaded rod which was used for the piston, the individual magnet holders are pressed together. A simulation like shown in figure 16 for the piston was not done because the force is dramatically lower. It was even possible to push the upper magnet holder all the way down without extraordinary effort. It can be estimated that the force at this point was about 300 N.

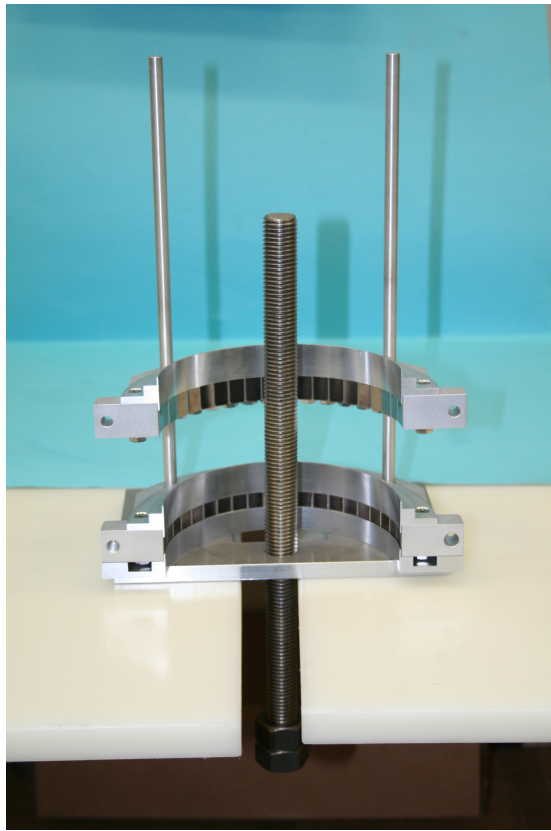


Figure 19: Construction of outer ring. The upper magnet holder levitates by the magnetic repulsion. It is held axially in position by two aluminum rods.

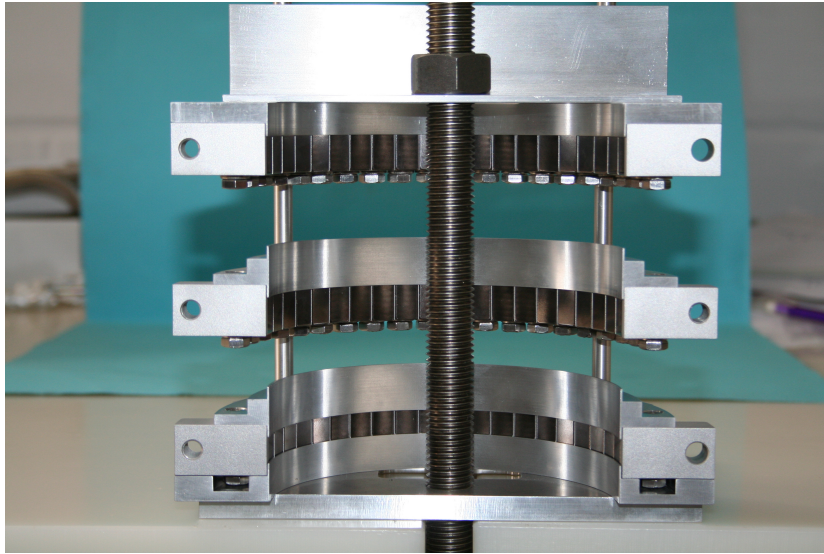


Figure 20: The upper and middle magnet holder levitate over the the bottom one. The big nut on the aluminum plate at the top is used to press them together.

3.5.4 Mounting the outer magnets around the tube

In this chapter the mounting of the outer half-rings around the tube with the piston inside will be described. Due to the high forces this is a non-trivial process. For this reason the assembling was tested around a test tube with a yet unsealed piston. To prevent damaging the tube, the half-ring itself or the piston a controlled method for a slow approach is needed. Therefore an assembly was designed and built to attach the half-rings on the tube.

During the design of the half-rings this method was already considered, which led to some specialties which will be covered in this chapter.

The initial decision which had to be made was if the half rings should be placed around the tube first and then the piston pressed in from the side. Or, if it was better to attach the half-rings with the piston already inside. The first method would make the attachment of the half-rings easy because the interaction of the magnets is comparatively small against the coupling to the piston. However, after this rather easy step it would be necessary to bring the piston in afterwards. Then it had to be dealt with alternating forces in the magnitude of more than 2500 N as the simulation (fig 13) in 3.4 showed.

The second method avoids this by having the piston already inside the tube. However the approach of the half-rings have to be controlled because there will be an attracting force towards the piston.

Both methods have their advantages and disadvantages. The reasons why the latter method was chosen are because we wanted to avoid the high forces which would be needed to bring the piston in. Especially the flipping direction of force seemed to be a possibly unsafe action. Furthermore, as the outer ring and the piston need to be separated from the test tube, this procedure had to be done again in the opposite direction.

base plate which holds the piston with an M20 threaded rod on its place. On

the ends of the piston, spacers are put to keep the test tube axially aligned. This is shown in figure 21.

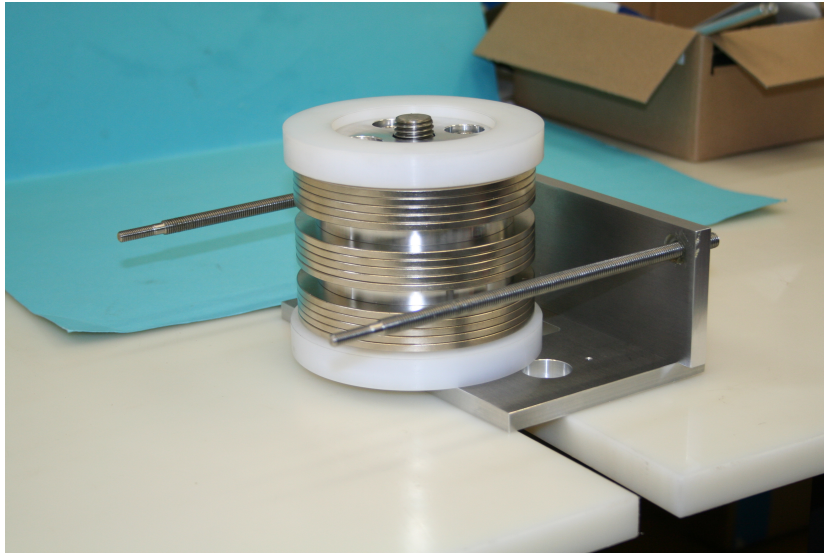


Figure 21: The piston is held by an M20 threaded rod from the bottom. The white spacers guarantee the right distance for the tube. The vertical plate is fixed to the bottom plate.

Then the tube is put over the piston. The first half-ring is now placed on a separate plate to equalize the height of the piston and the two threaded rods. This is shown in figure 22. The holes of this particular center magnet holder are smaller than the threaded rod. Only the first few centimeters can fit through this hole. This can also be seen in 21. This prevents a unintentionally movement towards the piston. By turning the nuts in front of the picture counterclockwise the threaded rod moves the half-ring towards the tube. When the half-ring is nearly at its supposed position, a similar spacer ring as for the piston is put over the tube to ensure the right distance. Then the threaded rods can be turned out completely and the vertical plate can be removed as well. The half-ring stays at its position only by magnetic coupling to the piston now (see figure 23).



Figure 22: The first half ring can slide towards the tube by turning the two double nuts at the vertical plate counterclockwise.



Figure 23: The first half ring is now on the tube. For the right distance, plastic spacers are put over the tube.

The approach for the next half-ring is similar to the first. Now the first ring stays at its position and the second moves towards the tube by turning the threaded rods. This is shown in figure 24. Unlike the first half-ring the center magnet holder has a threading for the threaded rod. Apart from that the half-rings are identical.

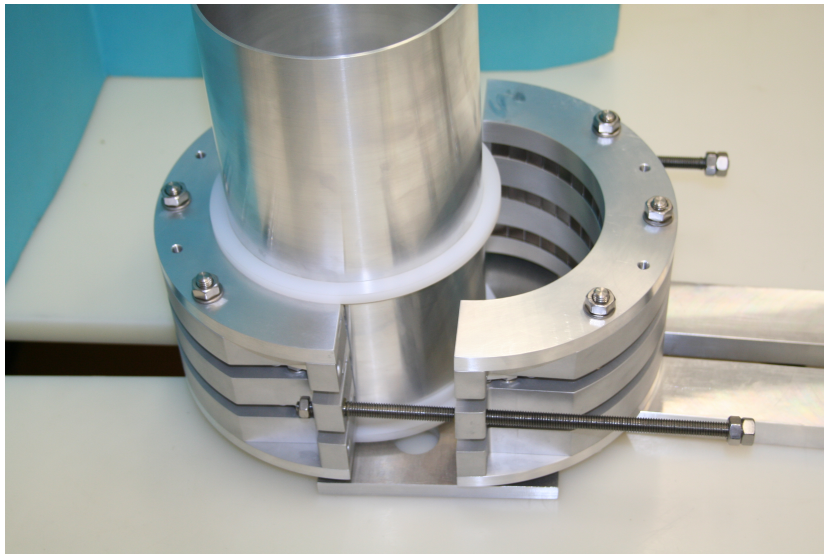


Figure 24: The second half-ring can again slide towards the tube by turning the threaded rods.

The last step is rather easy. After the full approach the half-rings are screwed together by 4 M8 screws as can be seen in figure 25. Everything that is then left to do is removing the M20 threaded rod from the piston.

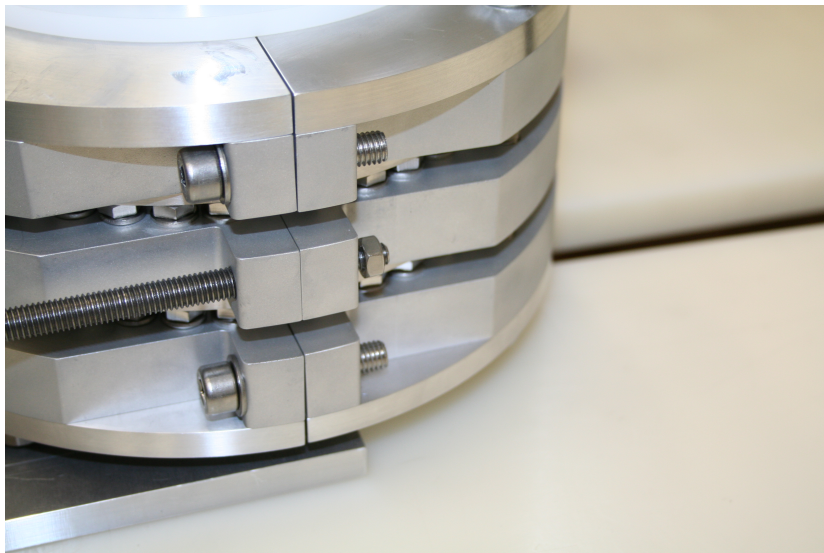


Figure 25: The half-rings are screwed together by 4 M8 bolts. Then the threaded rods are replaced by two M6 bolts. After tightening these screws the gaps closed.

This construction worked flawlessly for this test build, but it cannot be adopted to the final pump as is. The sealed piston won't have a M20 hole inside which can be used to fix it inside the final tube. Therefore the base plate/vertical plate

construction has to be changed for the final pump. As long as the threaded rods are fixed to something and an uncontrolled approach of the first half-ring is thereby prevented, any solution should be possible. However, the piston inside the tube must already be at the approximately right position. This needs to be ensured because otherwise the problems would occur which had been described at the beginning of this chapter.

3.6 Future construction

For this pump, the essential parts of the piston and outer ring are built. The remaining design of the pump contains the construction of the cylinder, the gas lines, and the drive.

The design of the cylinder, with the flanges at the end is shown in 26. Inside the front flange, the inlet and discharge lines can be seen. Flapper valves (brown) ensure only one directional flow. Piston and outer ring are also shown.

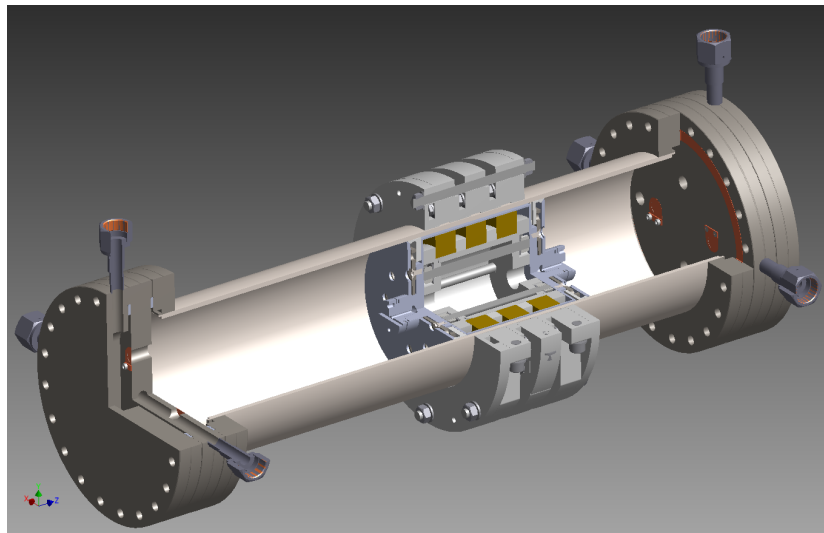


Figure 26: CGI cut view of the pump with cylinder and flanges attached.

With gas lines attached, the final pump may look like shown in 27. As the drive is not yet chosen, it is not shown.

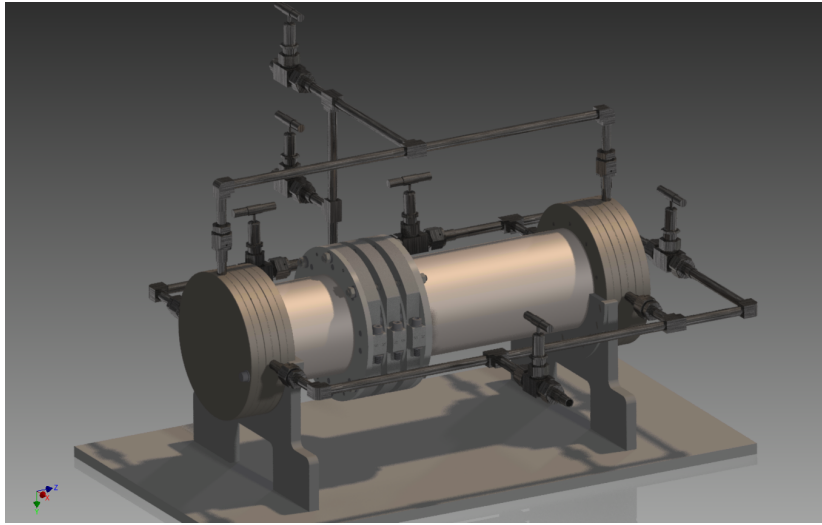


Figure 27: CGI view of the pump with gas lines attached.

4 Measurement of force

In chapter 3.4 we saw the simulated repulsion force (Fig. 13). In order to verify the result a test setup was built in Münster. The aim was to find out, which forces can be expected which will directly lead to predictions for the performance. In this chapter the construction and test will be presented.

4.1 Building a test setup

As the simulation showed forces up to more than 2500 N can be expected. In order to measure these forces a measurement tool has to be found. This already leads to the question if the piston should be pushed or pulled. In both cases the piston will be displaced while the outer ring is fixed. The displacement and associated force will then be measured. In the case of pushing a load cell would be needed which measures the force pressing between its top and bottom. In case of pulling a crane weighing cell can be put between a crane, or similar tool that can lift about 300 kg, and the piston. Mainly because a crane weighing cell was available the latter option was chosen.

The setup is rather simple. As shown in figure 28 it basically consists out of a frame of Kanya profiles. The outer ring is fixed to the plate which is connected to the frame. The force will be applied to the ring nut at the top. To prevent a shootout of the piston by the already discussed flipping direction of force at more than 30 mm displacement, a smaller safety plate was attached at the top of the frame. If the piston is pulled too high the center nut on the threaded rod will push against this plate and prevent further upward movement. The plastic spacers between the tube and the piston were fixed by nuts to the threaded rod as well, so that they cannot move during the displacement.



Figure 28: Test setup for the force measurement

For the lifting a fork lift was used as you can see in figure 29. The lower forks keep the frame on the ground because otherwise the whole frame would lift off. The crane weigher which was used is a *PCE-CS 1000* from *PCE Instruments*[13]. It has a 0.1 kg resolution. The forklift was able to lift in steps of nearly 1 mm. As the lashing strap is flexible it was especially at small displacements even easier to change the displacement precisely. However beyond the maximum force at 15 mm it was not possible to control the displacement accurately. The forklift was not able to move in small steps up while the force decreases. Therefore only the left flank of the curve could be measured. The displacement was measured between the center nut and the safety plate with a caliper.



Figure 29: Test setup with forklift and crane weighing cell near the maximum force.

4.2 Comparison of simulation and measurement

In the previous section the test setup was described. The result of the measurement is shown in figure 30. The shape of the curve is equal to the simulation. Both curves have a maximum at 15 mm. Resulting from the maximum force of 2500 N the maximum differential pressure will be 1.97 bar.

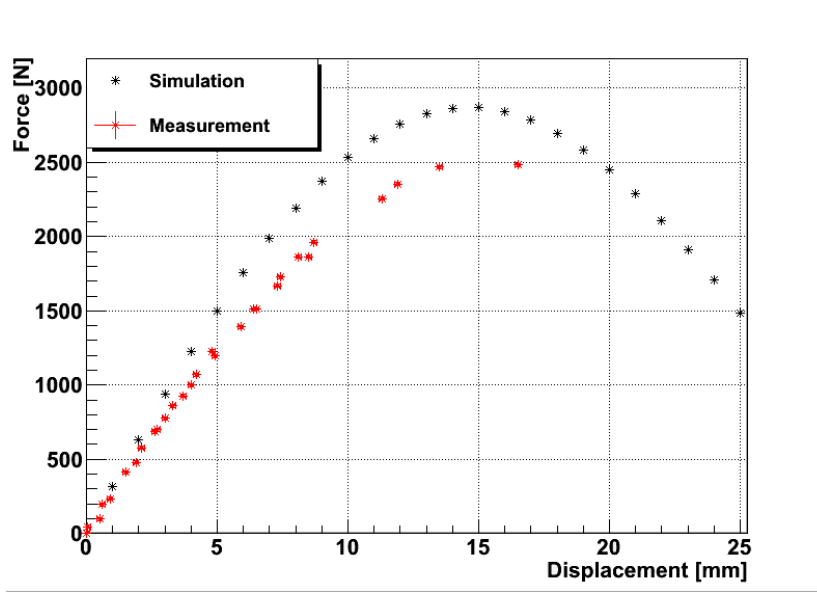


Figure 30: Simulated restoring force and measurement a given displacement.

The curve of the measurement is systematically lower than the simulation. The cause for this difference can be several reasons. The first is that the gaps between the magnets can may differ from the drawings. This would of course affect the result negatively, since the force strongly depends on the gap sizes. Especially if the gap in r direction differs from the drawing, the effect is considerable. Friction to the tube could also have an effect but that would rather increase the needed force than decreasing it. The own weight of the piston and everything that was attached to it has for sure a negative influence as well. Another reason might be that the magnetic dipole approximation is insufficient. When the dipole is not orientated exactly in the z -direction the field strength of 1.38 T is effectively lower. Also the nickel coating can - depending on its depth - reduce the volume of the magnetic material⁷. One thing that was already remarked at the unboxing of the magnets was that they have some imprecision in size. In this context samples of the magnets were measured again and it pointed out that all measured bar magnets are at least 0.1 mm smaller in each dimension at they are supposed to be. The ring magnets also have different thicknesses. In one ring thicknesses between 3.7 an 3.9 mm were measured. If all these aspects are taken into account the simulation looks like in figure 31.

The assumptions that were made are the following. The length of the bar magnets are set to 19.7 mm in height and 9.8 mm in length and width. The

⁷In fact Nickel is also ferromagnetic, but it is compared to NdFeB alloys very weak

simulated field in COMSOL was changed. As the ring magnets were significantly thinner each stack was simulated with 19,0 mm thickness. The only gap that could reasonably be changed was between the magnet holders. It's notable that after the assembly of the half-rings there was a gap between the individual magnet holders of about 1 mm. Therefore a spacing between these have been estimated to be 0.1 mm bigger than specified. The own weight was also calculated into account. All in all this simulation fits the measurement nicely. The remaining gap of less than 100 N might be the result of underestimated assumptions.

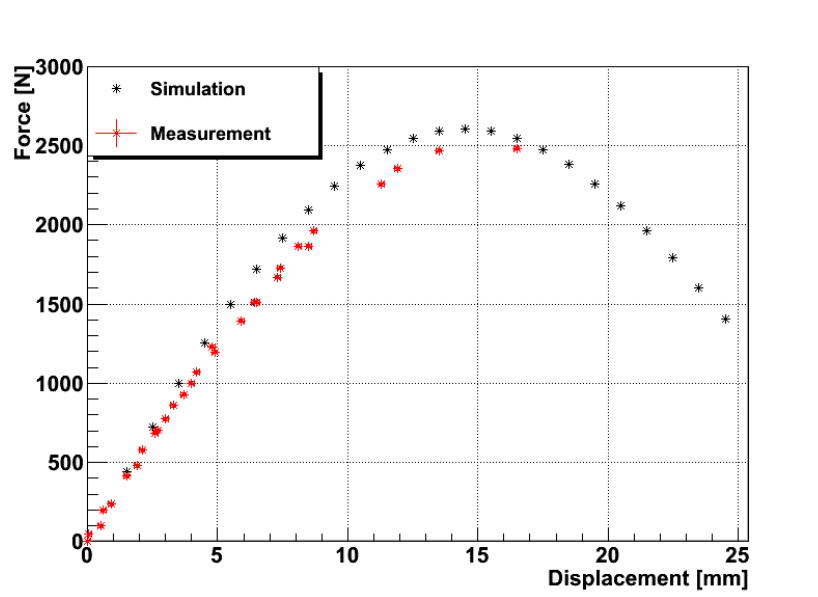


Figure 31: Simulated restoring force at a given displacement with some corrections.

5 Conclusion and Outlook

The aim of this work was to develop a magnetically driven piston pump which fulfills the vast requirements for recent high-purity experiments. At this point the results are very promising. Essential parts of a new pump have been built and tested. The demanded differential pressure of 2 bar is according to the measurement (fig. 30) complied. If the targeted aim of 100 slpm flow can be met, partly depends on the motor. This part has not been chosen yet, though. But with a cylinder capacity of about 5 l it will be very likely fulfilled. In any case the pump will easily outnumber the existing EXO-200 pump - in maximum differential pressure and flow. In addition, the design for the outer magnet ring makes it easy to exchange it with stronger magnets if necessary.

The estimated finishing date for the pump will be at the end of this year. At the moment the group in Stanford finishes the construction of the piston containers and the flanges to the tube. The design for the gas lines is being done in Münster.

When the pump is finished, further test will be done with the pump testing station to verify the maximum achievable differential pressure and flow. When the test are satisfying, the pump will be very likely to be used in nEXO and XENON1T.

All in all the design has to be rated as a success. The new magnet configuration resulted in a formidable improvement in coupling force, compared to the existing EXO-200 pump. As suggested in [7] a combination of radial and axial orientated magnets (i.e. Halbach array) may improve the coupling force further, but would be more difficult to construct. The high-purity requirements are ensured by a hermetic closed system, with only carefully selected parts, so that any intrinsic contamination is minimized. The risks of contamination, which encounter by malfunction of other types of pumps, cannot occur with this pump. Furthermore a long term reliable operation is ensured by a gasket design, which has been approved for a smaller, comparable pump.

References

- [1] Allen Bradley [ab.rockwellautomation.com/drives/powerflex 700](http://ab.rockwellautomation.com/drives/powerflex/700).
- [2] N. Ackerman, B. Aharmim, M. Auger, D. J. Auty, P. S. Barbeau, K. Barry, L. Bartoszek, E. Beauchamp, V. Belov, C. Benitez-Medina, M. Breidenbach, A. Burenkov, B. Cleveland, R. Conley, E. Conti, J. Cook, S. Cook, A. Coppens, I. Counts, W. Craddock, T. Daniels, M. V. Danilov, C. G. Davis, J. Davis, R. deVoe, Z. Djurcic, A. Dobi, A. G. Dolgolenko, M. J. Dolinski, K. Donato, M. Dunford, W. Fairbank, J. Farine, P. Fierlinger, D. Franco, D. Freytag, G. Giroux, R. Gornea, K. Graham, G. Gratta, M. P. Green, C. Hägemann, C. Hall, K. Hall, G. Haller, C. Hargrove, R. Herbst, S. Herrin, J. Hodgson, M. Hughes, A. Johnson, A. Karelin, L. J. Kaufman, T. Koffas, A. Kuchenkov, A. Kumar, K. S. Kumar, D. S. Leonard, F. Leonard, F. LePort, D. Mackay, R. MacLellan, M. Marino, Y. Martin, B. Mong, M. Montero Díez, P. Morgan, A. R. Müller, R. Neilson, R. Nelson, A. O'dian, K. O'Sullivan, C. Ouellet, A. Piepke, A. Pocar, C. Y. Prescott, K. Pushkin, A. Rivas, E. Rollin, P. C. Rowson, J. J. Russell,

- A. Sabourov, D. Sinclair, K. Skarpaas, S. Slutsky, V. Stekhanov, V. Strickland, M. Swift, D. Tosi, K. Twelker, P. Vogel, J.-L. Vuilleumier, J.-M. Vuilleumier, A. Waite, S. Waldman, T. Walton, K. Wamba, M. Weber, U. Wichoski, J. Wodin, J. D. Wright, L. Yang, Y.-R. Yen, and O. Ya. Zeldovich. Observation of two-neutrino double-beta decay in ^{136}Xe with the exo-200 detector. *Phys. Rev. Lett.*, 107:212501, Nov 2011.
- [3] E. Aprile and T. Doke. Liquid xenon detectors for particle physics and astrophysics. *Reviews of Modern Physics*, 82:2053–2097, July 2010.
- [4] E. Aprile and XENON1T collaboration. The XENON1T Dark Matter Search Experiment. *ArXiv e-prints*, June 2012.
- [5] M. Auger, D. J. Auty, P. S. Barbeau, L. Bartoszek, E. Baussan, E. Beauchamp, C. Benitez-Medina, M. Breidenbach, D. Chauhan, B. Cleveland, R. Conley, J. Cook, S. Cook, A. Coppens, W. Craddock, T. Daniels, C. G. Davis, J. Davis, R. deVoe, A. Dobi, M. J. Dolinski, M. Dunford, W. Fairbank, Jr., J. Farine, P. Fierlinger, D. Franco, G. Giroux, R. Gornea, K. Graham, G. Gratta, C. Hagemann, C. Hall, K. Hall, C. Hargrove, S. Herrin, J. Hodgson, M. Hughes, A. Karelin, L. J. Kaufman, J. Kirk, A. Kuchenkov, K. S. Kumar, D. S. Leonard, F. Leonard, F. LePort, D. Mackay, R. MacLellan, M. Marino, K. Merkle, B. Mong, M. Montero Díez, A. R. Müller, R. Neilson, A. Odian, K. O’Sullivan, C. Ouellet, A. Piepke, A. Pocar, C. Y. Prescott, K. Pushkin, A. Rivas, E. Rollin, P. C. Rowson, A. Sabourov, D. Sinclair, K. Skarpaas, S. Slutsky, V. Stekhanov, V. Strickland, M. Swift, D. Tosi, K. Twelker, J.-L. Vuilleumier, J.-M. Vuilleumier, T. Walton, M. Weber, U. Wichoski, J. Wodin, J. D. Wright, L. Yang, and Y.-R. Yen. The EXO-200 detector, part I: detector design and construction. *Journal of Instrumentation*, 7:5010, May 2012.
- [6] M. Auger, D. J. Auty, P. S. Barbeau, E. Beauchamp, V. Belov, C. Benitez-Medina, M. Breidenbach, T. Brunner, A. Burenkov, B. Cleveland, S. Cook, T. Daniels, M. Danilov, C. G. Davis, S. Delaquis, R. deVoe, A. Dobi, M. J. Dolinski, A. Dolgolenko, M. Dunford, W. Fairbank, Jr., J. Farine, W. Feldmeier, P. Fierlinger, D. Franco, G. Giroux, R. Gornea, K. Graham, G. Gratta, C. Hall, K. Hall, C. Hargrove, S. Herrin, M. Hughes, A. Johnson, T. N. Johnson, A. Karelin, L. J. Kaufman, A. Kuchenkov, K. S. Kumar, D. S. Leonard, F. Leonard, D. Mackay, R. MacLellan, M. Marino, B. Mong, M. Montero Díez, A. R. Müller, R. Neilson, R. Nelson, A. Odian, I. Ostrovskiy, K. O’Sullivan, C. Ouellet, A. Piepke, A. Pocar, C. Y. Prescott, K. Pushkin, P. C. Rowson, J. J. Russell, A. Sabourov, D. Sinclair, S. Slutsky, V. Stekhanov, T. Tolba, D. Tosi, K. Twelker, P. Vogel, J.-L. Vuilleumier, A. Waite, T. Walton, M. Weber, U. Wichoski, J. Wodin, J. D. Wright, L. Yang, Y.-R. Yen, and O. Y. Zeldovich. Search for Neutrinoless Double-Beta Decay in Xe^{136} with EXO-200. *Physical Review Letters*, 109(3):032505, July 2012.
- [7] Ethan Brown. Magnet configuration simulations for a high pressure differential magnetically driven piston pump. Technical report, Institut für Kernphysik, University of Münster, 2012.

- [8] O. Buchmueller, R. Cavanaugh, D. Colling, A. De Roeck, M. J. Dolan, J. R. Ellis, H. Flächer, S. Heinemeyer, G. Isidori, D. Martínez Santos, K. A. Olive, S. Rogerson, F. J. Ronga, and G. Weiglein. Supersymmetry and dark matter in light of LHC 2010 and XENON100 data. European Physical Journal C, 71:1722, August 2011.
- [9] D. Clowe, M. Bradač, A. H. Gonzalez, M. Markevitch, S. W. Randall, C. Jones, and D. Zaritsky. A Direct Empirical Proof of the Existence of Dark Matter. apjl, 648:L109–L113, September 2006.
- [10] <http://www.hkcm.de>.
- [11] <http://www.Kanya.com>.
- [12] <http://www.mksinst.com>.
- [13] http://www.pce_instruments.com.
- [14] <http://www.swagelok.com>.
- [15] Christian Huhmann. engineer at University of Münster.
- [16] D. S. Leonard, P. Grinberg, P. Weber, E. Baussan, Z. Djurcic, G. Keefer, A. Piepke, A. Pocar, J.-L. Vuilleumier, J.-M. Vuilleumier, D. Akimov, A. Bellerive, M. Bowcock, M. Breidenbach, A. Burenkov, R. Conley, W. Craddock, M. Danilov, R. Devoe, M. Dixit, A. Dolgolenko, I. Ekhtout, W. Fairbank, J. Farine, P. Fierlinger, B. Flatt, G. Gratta, M. Green, C. Hall, K. Hall, D. Hallman, C. Hargrove, R. Herbst, J. Hodgson, S. Jeng, S. Kolkowitz, A. Kovalenko, D. Kovalenko, F. Leport, D. Mackay, M. Moe, M. Montero Díez, R. Neilson, A. Odian, K. O’Sullivan, L. Ounalli, C. Y. Prescott, P. C. Rowson, D. Schenker, D. Sinclair, K. Skarpaas, G. Smirnov, V. Stekhanov, V. Strickland, C. Virtue, K. Wamba, and J. Wodin. Systematic study of trace radioactive impurities in candidate construction materials for EXO-200. Nuclear Instruments and Methods in Physics Research A, 591:490–509, July 2008.
- [17] F. Leport, R. Neilson, P. S. Barbeau, K. Barry, L. Bartoszek, I. Counts, J. Davis, R. Devoe, M. J. Dolinski, G. Gratta, M. Green, M. M. Díez, A. R. Müller, K. O’Sullivan, A. Rivas, K. Twelker, B. Aharmim, M. Auger, V. Belov, C. Benitez-Medina, M. Breidenbach, A. Burenkov, B. Cleveland, R. Conley, J. Cook, S. Cook, W. Craddock, T. Daniels, M. Dixit, A. Dobi, K. Donato, W. Fairbank, J. Farine, P. Fierlinger, D. Franco, G. Giroux, R. Gornea, K. Graham, C. Green, C. Hägemann, C. Hall, K. Hall, D. Hallman, C. Hargrove, S. Herrin, M. Hughes, J. Hodgson, F. Juget, L. J. Kaufman, A. Karelin, J. Ku, A. Kuchenkov, K. Kumar, D. S. Leonard, G. Lutter, D. Mackay, R. MacLellan, M. Marino, B. Mong, P. Morgan, A. Odian, A. Piepke, A. Pocar, C. Y. Prescott, K. Pushkin, E. Rollin, P. C. Rowson, B. Schmoll, D. Sinclair, K. Skarpaas, S. Slutsky, V. Stekhanov, V. Strickland, M. Swift, J.-L. Vuilleumier, J.-M. Vuilleumier, U. Wichoski, J. Wodin, L. Yang, and Y.-R. Yen. A magnetically driven piston pump for ultra-clean applications. Review of Scientific Instruments, 82(10):105114, October 2011.

- [18] www.comsol.com.
- [19] Xenon100 Collaboration, E. Aprile, K. Arisaka, F. Arneodo, A. Askin, L. Baudis, A. Behrens, E. Brown, J. M. R. Cardoso, B. Choi, D. Cline, S. Fattori, A. D. Ferella, K. L. Giboni, A. Kish, C. W. Lam, R. F. Lang, K. E. Lim, J. A. M. Lopes, T. Marrodán Undagoitia, Y. Mei, A. J. Melgarejo Fernandez, K. Ni, U. Oberlack, S. E. A. Orrigo, E. Pantic, G. Plante, A. C. C. Ribeiro, R. Santorelli, J. M. F. Dos Santos, M. Schumann, P. Shagin, A. Teymourian, E. Tziaferi, H. Wang, and M. Yamashita. The XENON100 dark matter experiment. *Astroparticle Physics*, 35:573–590, April 2012.
- [20] F. Zwicky. On the Red Shift of Spectral Lines through Interstellar Space. *Proceedings of the National Academy of Science*, 15:773–779, October 1929.
- [21] F. Zwicky. On the Masses of Nebulae and of Clusters of Nebulae. *apj*, 86:217, October 1937.

Danksagung

Vielen Dank möchte ich an dieser Stelle denen, die mich im Zuge dieser Arbeit unterstützt haben. Zunächst danke ich Prof. Weinheimer für die freundliche Aufnahme in die Arbeitsgruppe und für die Möglichkeit, zu diesem Projekt einen Teil beitragen zu dürfen. Es spannend, etwas für zwei herausragende Experimente geschaffen zu haben. Der gesamten Arbeitsgruppe danke ich für die mir für Fragen immer freundlich zur Verfügung standen.

Ein besonderer Dank geht an Christian Huhmann, der mich in die Bedienung von Autodesk Inventor eingewiesen hat und insbesondere auch sämtliche Konstruktionen mit designt und montiert hat. Nicht vergessen möchte ich hier die Feinmechanische Werkstatt für die Konstruktion der verschiedenen Einzelteile.

Einen ganz großen Dank spreche ich außerdem Ethan Brown aus, für die freundliche Betreuung in der Arbeitsgruppe und für das Korrekturlesen dieser Arbeit. Dies veranlasste mich erst diese Arbeit auf englisch zu verfassen.

Meinen Freunden in Münster danke ich für die tolle Zeit während des Bachelor Studiums. Ich hoffe die nächsten Jahre werden mindestens genauso fantastisch.

Zuletzt will ich meiner Familie danken, die mir das Studium ermöglicht und ohne deren Unterstützung ich nicht so weit gekommen wäre.

Plagiatserklärung des Studierenden

Hiermit versichere ich, dass die vorliegende Arbeit über "Design und Tests zum Bau einer magnetisch getriebenen Kolbenpumpe für Anwendungen in hochreinen Xenon-Experimenten" selbstständig verfasst worden ist, dass keine anderen Quellen und Hilfsmittel als die angegebenen benutzt worden sind und dass die Stellen der Arbeit, die anderen Werken – auch elektronischen Medien – dem Wortlaut oder Sinn nach entnommenen wurden, auf jeden Fall unter Angabe der Quelle als Entlehnung kenntlich gemacht worden sind.

(Datum, Unterschrift)

Ich erkläre mich mit einem Abgleich der Arbeit mit anderen Texten zwecks Auffindung von Übereinstimmungen sowie mit einer zu diesem Zweck vorzunehmenden Speicherung der Arbeit in eine Datenbank einverstanden.

(Datum, Unterschrift)